PHYSICAL REVIEW B **96**, 180305(R) (2017)

Phonon mode links ferroicities in multiferroic $[(CH_3)_2NH_2]Mn(HCOO)_3$

Kendall D. Hughey,[1] Amanda J. Clune,[1] Michael O. Yokosuk,[1] Amal al-Wahish,[1] Kenneth R. O'Neal,[1] Shiyu Fan,[2] Nandita Abhyankar,[3,4,5] Hongjun Xiang,[6,7] Zhiqiang Li,[4] John Singleton,[8] Naresh S. Dalal,[3,4] and Janice L. Musfeldt[1,2]

[1]*Department of Chemistry, University of Tennessee, Knoxville, Tennessee 37996, USA*

[2]*Department of Physics and Astronomy, University of Tennessee, Knoxville, Tennessee 37996, USA*

[3]*Department of Chemistry and Biochemistry, Florida State University, Tallahassee, Florida 32306, USA*

[4]*National High Magnetic Field Laboratory, Tallahassee, Florida 32310, USA*

[5]*Center for Nanoscale Science and Technology, National Institute of Standards and Technology, Gaithersburg, Maryland 20878, USA*

[6]*Key Laboratory of Computational Physical Sciences (Ministry of Education), State Key Laboratory of Surface Physics and Department of Physics, Fudan University, Shanghai 200433, People's Republic of China*

[7]*Collaborative Innovation Center of Advanced Microstructures, Nanjing 210093, People's Republic of China*

[8]*National High Magnetic Field Laboratory, Los Alamos National Laboratory, Los Alamos, New Mexico 87545, USA*

(Received 7 April 2017; revised manuscript received 14 April 2017; published 22 November 2017)

We combined magnetoinfrared spectroscopy, magnetization, and lattice dynamics calculations to explore the phase transitions in multiferroic $[(CH_3)_2NH_2]Mn(HCOO)_3$. Both the 185 K ferroelectric transition and the magnetically driven transition to the fully saturated state at 15.3 T involve the formate bending mode, direct evidence of a common connection between the two types of ferroicities and for how lattice distortions promote high-temperature magnetoelectric coupling in this system.

DOI: 10.1103/PhysRevB.96.180305

I. INTRODUCTION

Though challenging to realize [1–4], multiferroics offer fascinating opportunities to investigate coupling between electric polarization and magnetization (and vice versa) across broad energy and time scales. $[(CH_3)_2NH_2]Mn(HCOO)_3$ attracted our attention as a highly tunable molecule-based multiferroic with which to test the mechanistic aspects of these interactions [5,6]. This perovskitelike material has a metal-organic framework [Fig. 1(a)] and uses hydrogen bonds to stabilize flexible guest-host structures that drive order-disorder processes to achieve electric order [6,7]. In this system, $T_C = 185$ K, below which the ferroelectric polarization P is 1.5 $\mu C/cm^2$; ferroelectric domain walls have been visualized [6,8,9]. The low-temperature antiferromagnetic state ($T_N = 8.5$ K) is noncollinear and arises from the noncentrosymmetric nature of the formate bridge [6,10–14]. Curiously, cross coupling between the electric and magnetic orders [8,15,16] extends to relatively high temperatures [8,9], demonstrating that a low ordering temperature may not be a barrier to strong magnetoelectric coupling—although the precise mechanism for this effect has not yet been resolved. Magnetic field drives the system through a spin-flop transition at 0.31 T and into the fully saturated magnetic state at 15.3 T [17]. These energy scales are summarized in Fig. 1(b). In addition to representing a class of relatively unexplored multiferroics with flexible molecular architectures, the experimentally accessible transition temperatures and critical fields in $[(CH_3)_2NH_2]Mn(HCOO)_3$ [6,17] are ideal for exploring the interplay between charge, structure, and magnetism. In this work, we unveil an unusual signature of this interaction: a phonon that is sensitive to the development of both electric and magnetic polarizations.

In order to explore what might control these ferroicities and the mechanisms that underlie the field-dependent properties above T_N [8,9], we measured the infrared vibrational response of $[(CH_3)_2NH_2]Mn(HCOO)_3$ and compared our findings with complementary lattice dynamics calculations and prior magnetization measurements [17]. We find that doublet splitting of the formate bending mode across T_C functions as a ferroelectric order parameter and that the same phonon mode is sensitive to

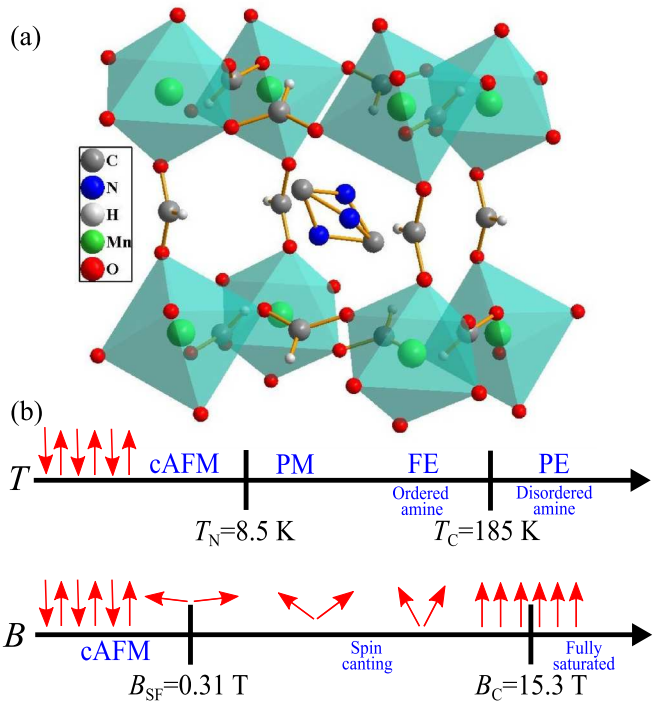

FIG. 1. (a) Crystal structure of $[(CH_3)_2NH_2]Mn(HCOO)_3$ showing the metal-formate framework and dynamically disordered dimethylammonium [6,10]. Ferroelectricity develops across the order-disorder transition [6,7]. The formate bridges define the Mn-O-C-O-Mn superexchange pathway ($J = -0.69$ K) [17,18]. (b) Summary of important temperature and magnetic energy scales [6,10,17]. PM = paramagnetic, cAFM = canted antiferromagnet, PE = paraelectric, FE = ferroelectric, B_{SF} = spin-flop field, and B_C = saturation field.

TABLE I. Frequencies and assignments for important modes in $[(CH_3)_2NH_2]Mn(HCOO)_3$ at 300 and 4 K. ν = symmetric stretching; ν_{as} = asymmetric stretching; ρ = rocking; δ = bending.

Mode assignments	ω 300 K (cm^{-1})	ω 4 K (cm^{-1})
ν(Mn-O_{eq})	292	296
$\delta(HCOO^-)$	794	794, 800
$\rho(NH_2)$	891	930
ν_{as}(CNC)	1025	1030
$\delta(NH_2)$	1632	1644

the development of the fully saturated magnetic state above 15.3 T. A single fundamental excitation in the form of a phonon thus underpins the development of the ferroic phases and magnetoelectric coupling—even though T_C and T_N are quite different. Similar lattice entanglements with charge and spin may provide a controlled route to enhanced coupling and high-temperature effects in other materials with coexisting electric and magnetic orders [12,13,19,20].

II. METHODS

$[(CH_3)_2NH_2]Mn(HCOO)_3$ single crystals were grown by solvothermal techniques [6] and mixed with paraffin (KBr) for transmittance in the far (mid) infrared, as required to control optical density. Grain sizes were on the order of 10 μm. We employed a series of Fourier transform spectrometers and an open flow cryostat (20–5000 cm^{-1}; 4.2–300 K). Absorption was calculated as $\alpha(\omega) = -\frac{1}{hd}\ln[\mathcal{T}(\omega)]$, where $\mathcal{T}(\omega)$ is the measured transmittance, h is the loading, and d is the thickness. Magnetoinfrared spectroscopy was performed at the National High Magnetic Field Laboratory using a 35 T resistive magnet. Absorption differences were calculated as $\Delta\alpha = \alpha(\omega, B) - \alpha(\omega, B = 0)$ to emphasize small spectral changes with magnetic field. Structural relaxations, energies, and lattice dynamics calculations were performed using density functional theory (DFT) plus the on-site repulsion (U) method [21] as implemented in VASP [22] to reveal structures in different magnetic states as well as mode assignments and displacement patterns. The on-site (U) and nearest-neighbor repulsion (V) are set to standard values of 4 and 1 eV for Mn, respectively. The electron-ion interactions were treated using the projected augmented wave method [23].

III. RESULTS AND DISCUSSION

Figure 2(a) displays the infrared response of $[(CH_3)_2NH_2]Mn(HCOO)_3$ at 300 K. We assign the spectral features via comparison with chemically similar materials and complementary dynamics calculations [16,24–26]. Localized counterion and ligand modes resonate above 600 cm^{-1} and more collective, manganese-related features appear below 300 cm^{-1}. Table I summarizes the behavior of several key modes. The 794 cm^{-1} peak, assigned here as a formate bend, is of special importance because, as we shall see, it underlies the development of both polarization and magnetic saturation.

Figure 2(b) displays a closeup view of the 794 cm^{-1} formate bending mode. This feature breaks into a strong doublet across the 185 K order-disorder transition due to

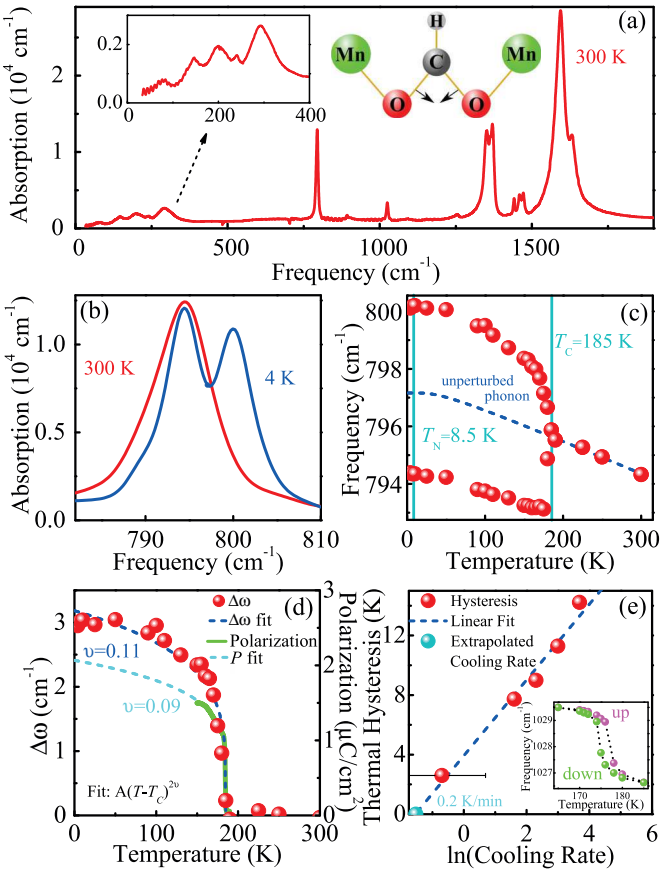

FIG. 2. (a) Infrared response of $[(CH_3)_2NH_2]Mn(HCOO)_3$ at room temperature and displacement pattern of formate bending mode. Inset: Low-frequency region of the spectra which has mostly Mn-containing modes. (b) Closeup view of the infrared-active formate bending mode. (c) Frequency vs temperature plot that reveals doublet splitting of the formate bending mode across T_C. An anharmonic fit of the high-temperature data points reveals the behavior of the unperturbed phonon [27]. Error bars are on the order of the symbol size. (d) Splitting of the formate bending mode vs temperature, a power law fit to this data, and polarization from Ref. [8]. (e) Width of the hysteresis around T_C vs cooling rate. The loop closes when the cooling rate is $<\approx$0.2 K/min. Inset: Hysteresis of the C-N-C asymmetric bending mode at 0.5 K/min.

the formation of two different types of hydrogen bonds between $(CH_3)_2NH_2^+$ and the formate ligands. The splitting is 6 cm^{-1}—large for an order-disorder ferroelectric. Additional fine structure, due to the development of three unique Mn-O-C-O-Mn superexchange pathways at low temperature, might be anticipated but is not resolved in $[(CH_3)_2NH_2]Mn(HCOO)_3$ due to bond length similarities [24]. Figure 2(c) shows peak position versus temperature. A fit to the data above T_C characterizes traditional anharmonic effects and is included for reference [27]. Below T_C, the fit represents the unperturbed phonon response (i.e., what would be expected in the absence of the transition). Figure 2(d) displays the splitting of the formate bending mode plotted as a difference between the high-frequency branch and the aforementioned anharmonic fit. The experimental polarization from Ref. [8] is included as well. The coincidence of the two data sets demonstrates that

the doublet splitting of the formate bending mode functions as an order parameter for the ferroelectric transition. A power law fit of the form $A(T_C - T)^{2\nu}$ reveals a critical exponent (ν) of 0.11—clearly different from mean field behavior (0.25) and suggestive of a more quasi-two-dimensional system [28]. The latter may lead to interesting applications in layered microelectronics. A ν of 0.11 is also in reasonable agreement with that obtained from fits to the polarization. The latter has more points around T_C and fewer at low temperature [8]. As shown in Fig. 2(e), the hysteresis around the ferroelectric transition closes with decreasing sweep rate.

We now turn to the spectroscopic response across the magnetically driven transition. Figure 3(a) displays a closeup view of the absorption of $[(CH_3)_2NH_2]Mn(HCOO)_3$ near the formate bending mode along with the absorption difference spectra, $\Delta\alpha(\omega, B) = \alpha(\omega, B = 35\ \mathrm{T}) - \alpha(\omega, B = 0\ \mathrm{T})$. Changes are on the order of 3% at full field. Figure 3(b) illustrates the development of the absorption difference with increasing magnetic field. Clear features are apparent even when the field is small. They grow with increasing field and saturate near $B_C = 15.3$ T. The derivativelike shape of $\Delta\alpha$ is consistent with a field-induced hardening of the underlying doublet. Importantly, only one phonon—the relatively soft formate (O-C-O) bending mode—changes in field. Recent calculations reveal that there is significant spin density on the oxygen centers of the formate ligands (and on Mn) [17], making this portion of the framework a logical candidate for spin-lattice coupling. There are no other field-induced local lattice distortions within our sensitivity. This includes the amine-related displacements as evidenced by the spectra in Fig. 3(c) in which the C-N-C asymmetric stretch is rigid. We therefore conclude that dimethylammonium plays no role in the magnetically driven transition at B_C. This is consistent with the lack of spin density on the counterion [17].

To quantify these effects, we integrate the absolute value of the field-induced absorption difference over a small energy window ($\int |\alpha(B) - \alpha(0)|\mathrm{d}\omega$) [29] and plot these values—along with magnetization [17] and the square of the magnetization—as a function of applied field. As shown in Fig. 3(d), changes in the formate bending mode track $[M(B)]^2$ [30]. The structure grows with increasing field and plateaus above 15.3 T, an indication that the lattice is sensitive to the microscopic nature of the spin state. Similar trends are seen in other molecule-based magnets such as $Mn[N(CN)_2]_2$ [25]. It is well known that phonons respond to spin correlations as $\Delta\omega = \lambda\langle S_i \cdot S_j\rangle$, where λ is the spin-phonon coupling constant and $\langle S_i \cdot S_j\rangle$ is the nearest-neighbor spin-spin correlation function [31]. Based on the field-induced frequency shift (on the order of 0.1 cm^{-1}) and the limiting low-temperature value of $\langle S_i \cdot S_j\rangle \approx S^2 = (5/2)^2$, we estimate $\lambda \leqslant 0.1\ \mathrm{cm}^{-1}$—a natural consequence of the low energy scales in this system.

The involvement of the formate bending mode in the magnetically driven transition to the fully saturated state is striking because the same mode is sensitive to the development of the ferroelectric polarization. This observation suggests that the lattice may be connected with high-temperature magnetoelectric coupling [8,9]. The key to unraveling this puzzle is to recall that formate is the superexchange lig-

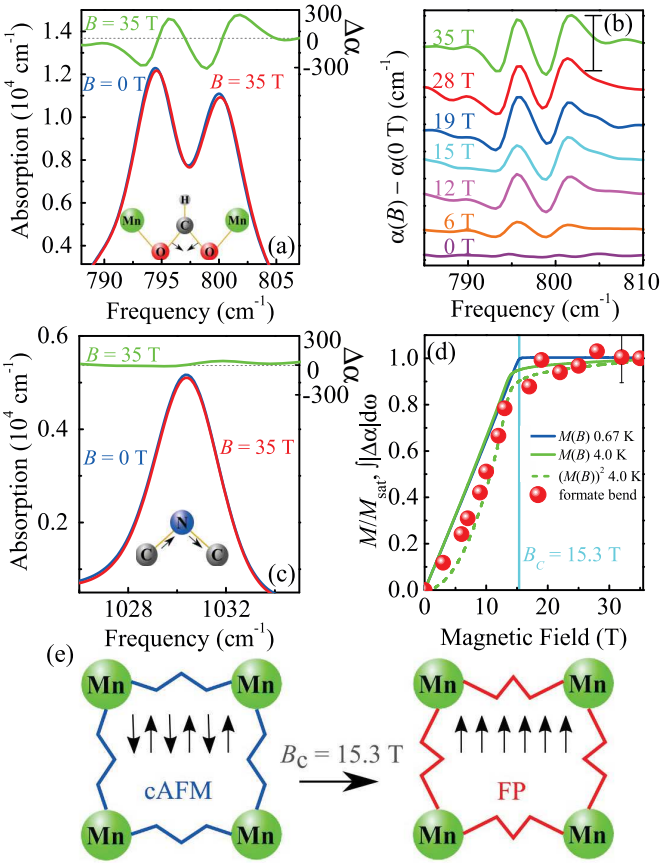

FIG. 3. (a) Closeup view of the absolute absorption spectrum focusing on the formate bending mode (displacement shown in schematic) at 0 and 35 T at 4.2 K along with the full field absorption difference spectrum. (b) Absorption difference spectra, $\Delta\alpha = \alpha(\omega, B) - \alpha(\omega, B = 0)$, showing field-induced changes in the formate bending mode for fields up to 35 T. The scale bar is 500 cm^{-1}. (c) Absorption spectrum of the 1030 cm^{-1} amine stretching mode at 0 and 35 T along with the full field absorption difference spectrum, revealing the lack of field dependence in the counterion mode. (d) Normalized magnetization [17], square of the magnetization, and integrated absorption difference as functions of applied field. (e) Schematic of the field-induced local lattice distortion of the formate ligand.

and. Interactions between Mn^{2+} centers thus take place via $Mn\cdots$formate$\cdots Mn$ exchange pathways [Fig. 1(a)]. Distortions of the superexchange pathway modify orbital overlap and therefore reduce J_{AFM}. This is because $J_{AFM} \sim -4t^2/U$, where t is the overlap integral ($\int \phi_1 H \phi_j \mathrm{d}\tau$). Reduction of J_{AFM} allows the fully polarized magnetic state to emerge at $B_C = 15.3$ T, somewhat lower than that expected from the zero field exchange energy.

Based on field-induced hardening of the formate bending mode and the Goodenough-Kanamori-Anderson rules stating a tendency toward a 90° superexchange angle in the ferromagnetic state [32], our data suggest that the O-C-O angle of the formate ligand decreases with increasing field, saturating only upon entry into the fully polarized state. We tested this supposition with density functional calculations, optimizing the structure in the antiferromagnetic and ferromagnetic

states. Our calculations confirm that the O-C-O bond angles in the ferromagnetic state are smaller than those in the antiferromagnetic state. Moreover, our calculations show that O displacement dominates this angular distortion—not C displacement. The greatest change in bond angle is 0.026° (from 123.635° in the antiferromagnetic state to 123.609° in the ferromagnetic state). Note that there are several different O-C-O angles in the system due to the low symmetry. This is shown schematically in Fig. 3(e). By way of comparison, a 1° out-of-plane bend in $[Cu(HF_2)(pyz)_2]BF_4$ is predicted to modify J_{AFM} by $\simeq 3\%$ [33].

$[(CH_3)_2NH_2]Mn(HCOO)_3$ is well suited to an analysis of structure-property relations. The molecular aspects of the metal-organic framework allows for synthetic variation, and the perovskitelike crystal structure makes this material topologically similar to the rare-earth manganites. The latter have attracted sustained attention for their incredibly complex P-T-B phase diagrams that sport multiple competing phases. In $HoMnO_3$, an applied magnetic field drives through five unique magnetic phases at 3 K before saturation [34]. By comparison, $[(CH_3)_2NH_2]Mn(HCOO)_3$ displays a strikingly simple B-T phase diagram in which magnetic field induces only a spin flop before magnetization saturates at 15.3 T [17]. This simplicity allows each transition to be isolated and explored in a straightforward manner. $[(CH_3)_2NH_2]Mn(HCOO)_3$ also behaves as a molecular material in that only one vibrational mode is sensitive to the change in the microscopic spin pattern [25,33]. This is quite different than what is observed in the multiferroic manganites, for instance, $DyMn_2O_5$, where the majority of phonon modes reveal a strong field dependence predominately associated with local distortions of the octahedra and square pyramids [35]. The same is true in $Sr_{1-x}Ba_xMnO_3$, where the large phonon changes at the ferroelectric and magnetic ordering transitions are characteristic of a displacive (rather than order-disorder) ferroelectric [36]. The behavior of the formate bending mode in $[(CH_3)_2NH_2]Mn(HCOO)_3$ is also quite different from an electromagnon which, although sensitive to the development of both electric and magnetic order in rare-earth manganites [37,38], is a collective (rather than elementary) excitation that naturally involves both spin and charge.

IV. CONCLUSION

In summary, $[(CH_3)_2NH_2]Mn(HCOO)_3$ is a rich platform for exploring the interplay between electric and magnetic polarizations in multiferroics, linked in this work by a single phonon. The latter is an infrared-active formate bending mode. Analysis of this structure across T_C shows that doublet splitting can be described in terms of a power law fit to the order parameter—just as polarization. The ligand bending mode also couples to the development of magnetization across B_C, a finding that we analyze in terms of how reduction of J_{AFM} facilitates the development of the fully saturated state. That a specific phonon mode underpins both ferroicities and magnetoelectric coupling is remarkable because T_C and T_N are quite different. This discovery opens the door to a significantly different research area in tunable low-energy-scale multiferroics.

ACKNOWLEDGMENTS

Research at Tennessee is supported by the National Science Foundation (DMR-1707846) and the Materials Research Fund at the University of Tennessee. A portion of this work was performed at the National High Magnetic Field Laboratory, which is supported by the National Science Foundation through DMR-1157490, the Department of Energy, and the State of Florida. J.S. appreciates funding from Basic Energy Sciences, U. S. Department of Energy FWP "Science in 100 T." H.X. was supported by NSFC (11374056), the Special Funds for Major State Basic Research (2015CB921700), Qing Nian Ba Jian Program, and Fok Ying Tung Education Foundation. N.S.D. is supported by NSF via CHE-1464955.

[1] N. A. Hill, J. Phys. Chem. B **104**, 6694 (2000).
[2] D. Khomskii, Physics **2**, 20 (2009).
[3] N. A. Benedek and C. J. Fennie, Phys. Rev. Lett. **106**, 107204 (2011).
[4] Y. Tokura, S. Seki, and N. Nagaosa, Rep. Prog. Phys. **77**, 076501 (2014).
[5] R. Ramesh, Nature (London) **461**, 1218 (2009).
[6] P. Jain, V. Ramachandran, R. J. Clark, H. D. Zhou, B. H. Toby, N. S. Dalal, H. W. Kroto, and A. K. Cheetham, J. Am. Chem. Soc. **131**, 13625 (2009).
[7] D. Di Sante, A. Stroppa, P. Jain, and S. Picozzi, J. Am. Chem. Soc. **135**, 18126 (2013).
[8] W. Wang, L. Q. Yan, J. Z. Cong, Y. L. Zhao, F. Wang, S. P. Shen, T. Zou, D. Zhang, S.-G. Wang, X.-F. Han, and Y. Sun, Sci. Rep. **3**, 2024 (2013).
[9] P. Jain, A. Stroppa, D. Nabok, A. Marino, A. Rubano, D. Paparo, M. Matsubara, H. Nakotte, M. Fiebig, S. Picozzi, E. S. Choi, A. K. Cheetham, C. Draxl, N. S. Dalal, and V. S. Zapf, npj Quantum Mater. **1**, 16012 (2016).
[10] X.-Y. Wang, L. Gan, S.-W. Zhang, and S. Gao, Inorg. Chem. **43**, 4615 (2004).
[11] X.-Y. Wang, Z.-M. Wang, and S. Gao, Chem. Commun. **0**, 281 (2008).
[12] P. J. Baker, T. Lancaster, I. Franke, W. Hayes, S. J. Blundell, F. L. Pratt, P. Jain, Z.-M. Wang, and M. Kurmoo, Phys. Rev. B **82**, 012407 (2010).
[13] K. Vinod, C. S. Deepak, S. Sharma, D. Sornadurai, A. T. Satya, T. R. Ravindran, C. S. Sundar, and A. Bharathi, RSC Adv. **5**, 37818 (2015).
[14] H. D. Duncan, M. T. Dove, D. A. Keen, and A. E. Phillips, Dalton Trans. **45**, 4380 (2016).
[15] Y. Tian, A. Stroppa, Y. Chai, L. Yan, S. Wang, P. Barone, S. Picozzi, and Y. Sun, Sci. Rep. **4**, 6062 (2014).
[16] M. Maczka, A. Gagor, B. Macalik, A. Pikul, M. Ptak, and J. Hanuza, Inorg. Chem. **53**, 457 (2014).
[17] A. J. Clune, K. D. Hughey, C. Lee, N. Abhyankar, N. S. Dalal, M.-H. Whangbo, J. Singleton, and J. L. Musfeldt, Phys. Rev. B **96**, 104424 (2017).

[18] A Hamiltonian of the form $H = -ZJ \sum_{\langle i,j\rangle_{xy}} S_i \cdot S_j - g\mu B \sum_i S_i^z$ is employed.

[19] L. C. Gómez-Aguirre, B. Pato-Doldán, J. Mira, S. Castro-García, M. A. Señarís-Rodríguez, M. Sánchez-Andújar, J. Singleton, and V. S. Zapf, J. Am. Chem. Soc. **138**, 1122 (2016).

[20] F.-R. Fan, H. Wu, D. Nabok, S. Hu, W. Ren, and A. Stroppa, J. Am. Chem. Soc. **139**, 12883 (2017).

[21] A. I. Liechtenstein, V. I. Anisimov, and J. Zaanen, Phys. Rev. B **52**, R5467 (1995); J. P. Perdew, K. Burke, and M. Ernzerhof, Phys. Rev. Lett. **77**, 3865 (1996).

[22] G. Kresse and J. Furthmüller, Comput. Mater. Sci. **6**, 15 (1996); Phys. Rev. B **54**, 11169 (1996).

[23] P. E. Blöchl, Phys. Rev. B **50**, 17953 (1994); G. Kresse and D. Joubert, *ibid.* **59**, 1758 (1999).

[24] M. Sánchez-Andújar, S. Presedo, S. Yáñez-Vilar, S. Castro-García, J. Shamir, and M. A. Señaís-Rodríguez, Inorg. Chem. **49**, 1510 (2010).

[25] T. V. Brinzari, P. Chen, Q.-C. Sun, J. Liu, L.-C. Tung, Y. Wang, J. A. Schlueter, J. Singleton, J. L. Manson, M.-H. Whangbo, A. P. Litvinchuk, and J. L. Musfeldt, Phys. Rev. Lett. **110**, 237202 (2013).

[26] K. Szymborska-Malek, M. Trzebiatowska-Gusowska, M. Maczka, and A. Gagor, Spectrochim. Acta Mol. Biomol. Spectrosc. **159**, 35 (2016).

[27] The anharmonic fit of the high-temperature data points follows the form $\omega = \omega_0 + C\{1 + 2/[\exp(0.144\omega_0/T) - 1]\}$, where ω_0 is 797.8 cm^{-1} and C is -0.6538.

[28] F. Kagawa, K. Miyagawa, and K. Kanoda, Nature (London) **436**, 534 (2005).

[29] By so doing, we generate a function that is proportional to the frequency shift but with significantly smaller error bars. We tested this method in prior work on $[Ru_2(O_2CMe)_4]_3[Cr(CN)_6]$. A comparison of the frequency shift and the absorption difference analysis shows that they are proportional, thus justifying our approach. T. V. Brinzari, P. Chen, L.-C. Tung, Y. Kim, D. Smirnov, J. Singleton, J. S. Miller, and J. L. Musfeldt, Phys. Rev. B **86**, 214411 (2012).

[30] E. Granado, A. García, J. A. Sanjurjo, C. Rettori, I. Torriani, F. Prado, R. D. Sánchez, A. Caneiro, and S. B. Oseroff, Phys. Rev. B **60**, 11879 (1999).

[31] J. H. Lee and K. M. Rabe, Phys. Rev. B **84**, 104440 (2011).

[32] J. B. Goodenough, *Magnetism and the Chemical Bond* (Wiley, New York, 1963).

[33] J. L. Musfeldt, L. I. Vergara, T. V. Brinzari, C. Lee, L. C. Tung, J. Kang, Y. J. Wang, J. A. Schlueter, J. L. Manson, and M.-H. Whangbo, Phys. Rev. Lett. **103**, 157401 (2009).

[34] B. Lorenz, ISRN Condensed Matter Phys. **2013**, 497073.

[35] J. Cao, L. I. Vergara, J. L. Musfeldt, A. P. Litvinchuk, Y. J. Wang, S. Park, and S.-W. Cheong, Phys Rev. Lett. **100**, 177205 (2008).

[36] V. Goian, F. Kadlec, C. Kadlec, B. Dabrowski, S. Kolesnik, O. Chmaissem, D. Nuzhnyy, M. Kempa, V. Bovtun, M. Savinov, J. Hejtmánek, J. Prokleška, and S. Kamba, J. Phys.: Condens. Matter **28**, 175901 (2016).

[37] A. B. Sushkov, Ch. Kant, M. Schiebl, A. M. Shuvaev, A. Pimenov, A. Pimenov, B. Lorenz, S. Park, S.-W. Cheong, M. Mostovoy, and H. D. Drew, Phys. Rev. B **90**, 054417 (2014).

[38] M. Schmidt, Ch. Kant, T. Rudolf, F. Mayr, A. A. Mukhin, A. M. Balbashov, J. Deisenhofer, and A. Loidl, Eur. Phys. J. B **71**, 411 (2009).